Acta Pharmaceutica Sinica B 2023;13(6):2765–2777

Chinese Pharmaceutical Association
Institute of Materia Medica, Chinese Academy of Medical Sciences

Acta Pharmaceutica Sinica B

www.elsevier.com/locate/apsb
www.sciencedirect.com

ORIGINAL ARTICLE

Novel discovery of schisandrin A regulating the interplay of autophagy and apoptosis in oligoasthenospermia by targeting SCF/c-kit and TRPV1 *via* biosensors

Lijuan Ma[a,†], Boyi Li[b,†], Jinchen Ma[b,†], Chunyuan Wu[c], Nan Li[a,e], Kailin Zhou[d], Yun Yan[b], Mingshuang Li[a], Xiaoyan Hu[a], Hao Yan[a], Qi Wang[b,*], Yanfei Zheng[b,*], Zhisheng Wu[a,e,*]

[a]*Beijing University of Chinese Medicine, School of Chinese Materia Medica, Beijing 100029, China*
[b]*Beijing University of Chinese Medicine, School of Traditional Chinese Medicine, Beijing 100029, China*
[c]*Shanghai New Asiatic Pharmaceuticals Hanjiang Co., Ltd., Yangzhou 225127, China*
[d]*Beijing University of Chinese Medicine, School of Humanities, Beijing 100029, China*
[e]*Engineering Research Center of Ministry of Education for Traditional Chinese Medicine Pharmaceutical and New Drug Development, Beijing 100029, China*

Received 11 October 2022; received in revised form 2 December 2022; accepted 3 January 2023

KEY WORDS

Oligoasthenospermia;
Male infertility;
Autophagy;
Apoptosis;
Biosensor;
Schisandrin A.

Abstract Oligoasthenospermia is the primary cause of infertility. However, there are still enormous challenges in the screening of critical candidates and targets of oligoasthenospermia owing to its complex mechanism. In this study, stem cell factor (SCF), c-kit, and transient receptor potential vanilloid 1 (TRPV1) biosensors were successfully established and applied to studying apoptosis and autophagy mechanisms. Interestingly, the detection limit reached 2.787×10^{-15} g/L, and the quantitative limit reached 1.0×10^{-13} g/L. Furthermore, biosensors were used to investigate the interplay between autophagy and apoptosis. Schisandrin A is an excellent candidate to form a system with c-kit similar to SCF/c-kit with a detection constant (K_D) of 5.701×10^{-11} mol/L, whereas it had no affinity for SCF. In addition, it also inhibited autophagy in oligoasthenospermia through antagonizing TRPV1 with a K_D of up to 4.181×10^{-10} mol/L. In addition, *in vivo* and *in vitro* experiments were highly consistent with the biosensor. In summary, high-potency schisandrin A and two potential targets were identified, through which schisandrin A could reverse the apoptosis

*Corresponding authors.
E-mail addresses: wangqi710@126.com (Qi Wang), yanfei_z@163.com (Yanfei Zheng), wzs@bucm.edu.cn (Zhisheng Wu).
[†]These authors made equal contributions to this work.
Peer review under the responsibility of Chinese Pharmaceutical Association and Institute of Materia Medica, Chinese Academy of Medical Sciences.

https://doi.org/10.1016/j.apsb.2023.01.004

caused by excessive autophagy during oligoasthenospermia. Our study provides promising insights into the discovery of effective compounds and potential targets *via* a well-established *in vitro-in vivo* strategy.

1. Introduction

The World Health Organization (WHO) estimates that 60 to 80 million couples are affected by infertility. In recent years, male infertility has increased significantly, accounting for 40%−50% of cases of infertility[1]. The most common cause of male infertility is decreased semen quality[2,3] with oligospermia and asthenospermia accounting for 58%−64% of these cases[4−6]. The Huangjing Zanyu capsule (New Drug Certificate: Z20010103) developed by us early, is the first national new drug of Chinese materia medica (CMM) for the treatment of male infertility in China. Since its listing in 2005, it has been proven to have a remarkable effect on male infertility caused by oligoasthenospermia and has been applied in over 1000 hospitals in 18 provinces and cities. Small molecules from CMM have been considered as candidates and critical quality attributes (CQAs). Exploring the active substances in CMM is essential for understanding its mechanism. And *vice versa*, active substances in CMM with clear clinical efficacy are essential for innovative pharmaceutical development[7−9]. Artemisinin[10,11] and icaritin[12], which have been developed as novel drugs, are two typical examples. Previous studies have shown that schisandrin A is an essential and curative CQA of Huangjing Zanyu Capsules based on serum pharmacochemistry analysis[13]. Schisandrin A is an essential CQA that modulates cell growth, differentiation, and fate determination under pathophysiological circumstances[14,15]. Therefore, we hypothesized that schisandrin A is the vital substance of Huangjing Zanyu Capsules for the treatment of oligoasthenospermia. However, the biological mechanisms have not yet been clearly explained.

Increasing evidence has linked oligoasthenospermia to autophagy and apoptosis. The regulation of apoptosis during cell death is unidirectional and is induced by intra- or intercellular mechanisms[16]. It can actively remove aging and abnormal cells in the body serving as a "scavenger"[17,18]. It is clear that the intracellular apoptosis signal typically activates the mitochondrial pathway, stimulating the activation of BH3-only protein to bind to B-cell lymphoma-2 (Bcl-2), and Bcl-2 assaciated X protein (Bax)/Bax to aggregate to the mitochondrial membrane[19,20]. Simultaneously, SCF/c-kit is closely related to the apoptosis of spermatogenic cells[21−23]. The SCF/c-kit signaling system plays a critical role in oligoasthenospermia[24−28]. Apoptosis-induced cell death is decisive; however, the impact of autophagy on cell death varies[29]. Autophagy and apoptosis share multiple regulatory proteins[30,31]. The complex interplay between them is significant for pathophysiology[32,33]. The interplay between autophagy and apoptosis influences the clearance of dysregulated cells as well as the occurrence and aggravation of some diseases[34,35]. Ca^{2+} is a significant regulator of autophagy and apoptosis[36]. Transient receptor potential vanilloid (TRPV) channels are highly Ca^{2+}-selective and play a vital role in regulating autophagy signaling[37−39]. Numerous studies have shown that TRPV can promote autophagy signaling by producing Ca^{2+} to inhibit Akt. Additionally, TRPV1 is a critical regulatory protein that cooperates with autophagy and apoptosis machineries[40,41]. Genetic deletion of TRPV1 results in increased basal levels of p62 as well as defective autophagic responses to mTOR inhibitors and the autophagy inducer rapamycin[42]. This indicates that disruption of the balance between autophagy and apoptosis has significant pathophysiological consequences.

However, the relationship between autophagy and apoptosis in oligoasthenospermia is not well defined. Various biochemical and morphological methods have been used in autophagy and apoptosis investigation[43]. Specifically, biochemical methods are unsuitable for rapid analysis. Additionally, morphological methods remain indispensable; however, they are neither facile nor time effective[44−46]. This suggests that the current bottleneck in the study of the relationship between autophagy and apoptosis lies in the real-time monitoring[47]. Therefore, a biosensor platform is an excellent choice. Typical commonly used research option is an alternative monitoring biosensor system for autophagy, which characterizes an assay based on the two-photon fluorescent biosensor[48]. The microfluidic chip (MC) device is another emerging technology favored for real-time monitoring of autophagy and apoptosis because of its three-dimensional (3D) environment suitable for cell co-culture[49,50]. In recent years, wide band gap III−V group semiconductor materials, such as GaAs, have emerged as promising candidates for biosensing applications[51,52]. The main advantage of III−V-based materials is their ability to resist harsh chemical environments (acidic or alkaline)[53], leading to enhanced sensor stability and reliability, such as in high electron mobility transistors (HEMT)[54]. Moreover, they have a spontaneous polarization field and piezoelectric polarization field, which forms a deep potential well at the interface. Surrounded electrons are confined to this well and form a high density of two-dimensional electron gas (2DEG)[55]. The 2DEG channel is highly sensitive to the surface charge distribution, which determines its ultrahigh sensitivity and applicability in complex systems[54]. Unlike conventional field-effect transistor (FET) sensors, in the gated HEMT structure, biomolecular receptors are immobilized on a gold gate electrode separated from the active region of the HEMT device[56].

In the present study, a high-sensitivity HEMT device was introduced to establish the SCF/c-kit biosensor and then applied creatively to the investigation of the apoptosis mechanism of schisandrin A intervention in oligoasthenospermia. Furthermore, a TRPV1 biosensor was constructed to explore the interplay between autophagy and apoptosis of schisandrin A intervention in

oligoasthenospermia. Finally, the *in vitro* and *in vivo* mechanisms were explored to further support that schisandrin A regulates autophagy and apoptosis in oligoasthenospermia. These biosensors can be used as promising tools for mechanistic investigation, providing efficient potential targets and candidates for oligoasthenospermia.

2. Materials and methods

2.1. Instruments and reagents

Schisandrin A (lot: PS000928) was purchased from BioRuler Corp (CT, USA). CMC-Na (lot: L13M8G35918) was obtained from Yuanye Bio-Technology Co., Ltd. (Shanghai, China). Methanol was purchased from Thermo Fisher Scientific Corp (MA, USA). Glucoside tripterygium wilfordine (GTW) and cyclophosphamide (ACR) were purchased from Shanghai Fudan Fuhua Pharmaceutical Co., Ltd. (Shanghai, China). Levocarnitine (lot: 01,161,202) was obtained from Merro Pharmaceutical Co., Ltd. (Dalian, China). Anhydrous ethanol, formaldehyde, glacial acetic acid, toluene, hematoxylin dye solution, eosmium tetroxide, acetone, hydrochloric acid, resin, and sodium hydroxide were purchased from the Beijing Chemical Works (Beijing, China). SCF protein and c-kit protein were provided by Zhongnongboxin Technology Co., Ltd. (Beijing, China). TRPV1 protein was provided by Shenzhen Crystalo Biopharmaceutical Co., Ltd. (Shenzhen, China).

2.2. Animal modeling and intervention for the autophagy and apoptosis mechanism exploration of schisandrin A

Fifty male SD rats (SPF, 170−190 g) obtained from Sibeifu (Beijing) Biotechnology Co., Ltd. (Certification No. SCXK-Jing-2011-0004) were housed in the Experimental Animal Center of Beijing University of Chinese Medicine (BUCM) (temperature at 22−24 °C and humidity at 52%−56%) with standard chow and water and 12 h light/dark cycle. Fifty rats were divided into four groups randomly as follows: 15 rats each were in the normal control (NS) and model (GTW)[57,58] groups and 10 each were in the levocarnitine group (Levo)[59,60] and schisandrin A group (WWZ). Among them, schisandrin A was the vital CQA of Huangjing Zanyu capsule (New Drug Certificate: Z20010103) identified by ultra-performance liquid chromatography with electrospray tandem mass spectrometry (UPLC−MS/MS) (Supporting Information). The specific dosing regimen of each group and the protocol for sperm quality examination[61] was placed on the Supporting Information.

The animal experiments have been approved by the ethical committee of BUCM (No. BUCM-4-2019112502-4067). All animal experiments were performed in accordance with relevant guidelines and regulations.

2.3. Cell culture, grouping and intervention for the autophagy and apoptosis mechanism exploration of schisandrin A

Spd2 cells were cultured in Dulbecco's modified eagle medium (DMEM) supplemented with 10% fetal bovine serum (FBS) and 1% Pen/Strep and grown in culture flasks (Corning) at 37 °C in a humidified 5% CO_2 atmosphere. The cell model was established by adding 1 mmol/L acrolein (ACR) into the culture medium[58,62]. The intervention was performed by giving 5, 10, 20 μmol/L of schisandrin A respectively after 3 h of modeling. After 48 h of intervention, the cells were carefully scraped off and collected into EP tubes for subsequent experiments. According to the instruction, CCK8 assay (CWBio, China) was performed to evaluate the vitality of cells.

2.4. The development of SCF, c-kit, and TRPV1 AlGaAs/GaAs HEMT biosensors

The AlGaAs/GaAs HEMT chip in this study was constructed by molecular beam epitaxy (MBE) on the GaAs substrate. Specifically, a 500 nm GaAs buffer layer was used as the foundation. Subsequently, a 15 nm $In_{0.3}Ga_{0.7}As$ channel layer, a 4 nm $Al_{0.3}Ga_{0.7}As$ spacer layer, a Si δ-doping layer, a 25 nm $Al_{0.3}Ga_{0.7}As$ barrier layer and a 30 nm GaAs cap layers was put on layer by layer. Then, a self-assembled monolayer was constructed by 0.1 mol/L 3-mercaptopropionic acid (3-MPA) for 24 h to format a layer of Au−S bonding on the Au surface of the HEMT sensor. A mixture of equivoluminal 20 mmol/L 1-(3-dimethylaminopropyl)-3-ethylcarbodiimide hydrochloride (EDC) and 50 mmol/L *N*-hydroxysuccinimide (NHS) was used to activate carboxyl of 3-MPA for 15 min. Finally, 100 μg/mL SCF, c-kit, or TRPV1 protein were incubated on the chip at 4 °C.

Scanning electron microscope (SEM) was applied to determine the immobilization of proteins. The drain-source current (I_{DS}-V_{DS}) was measured by ChI660E. The voltage was set as 2.0 V and the sampling rate as 10 ns? Bovine serum albumin (BSA) was introduced as control group to explore the interaction between SCF and c-kit. Furthermore, the ferulic acid was used as a negative control for the interaction between schsandrin A and c-kit. Moreover, according to the previous algorithms and investigation[54], the detection limit (DL), quantitation limit (QL), detection range, and specificity of biosensors were explored.

2.5. Autophagy and apoptosis mechanism exploration of schisandrin A by SCF, c-kit, and TRPV1 HEMT biosensors

Eleven concentrations of schisandrin A ranging from 0.1 pmol/L to 1.0 mmol/L were measured by the biosensors functionalized by SCF, c-kit, and TRPV1 respectively. 0.1 mol/L phosphate-buffered saline (PBS) solution was used as the control. Each test was repeated three times. Furthermore, the K_D was calculated according to Eqs. (1)−(3) [63]. Simultaneously, the interaction between SCF and c-kit was implemented by the c-kit HEMT biosensor.

$$\left[A_b\right] + \left[A_g\right] \leftrightarrow \left[A_b - A_g\right] \tag{1}$$

$$K = K_A = 1 \,/\, K_D = \left[A_b - A_g\right] \,/\, \left[A_b\right] \cdot \left[A_g\right] \tag{2}$$

$$\left[A_g\right] \,/\, \Delta I = \left[A_g\right] \,/\, \Delta I_{max} + K_D \,/\, \Delta I_{max} \tag{3}$$

where K is the equilibrium constant for Eq. (1). K_A is the association constant, and K_D is the dissociation constant. $[A_b]$ is the concentration of the unbound antibody (c-kit) immobilized on the sensor surface. $[A_g]$ is the component concentration (recorded as C). $[A_b - A_g]$ is the concentration of the antibody−component complex on the sensor surface. ΔI is the current change. The expression of ΔI was $\Delta I = I - I_0$, in which, I_0 was the current

generated by the blank solution and I was the current generated by the sample solution. ΔI_{max} is the saturated current change.

2.6. Molecular docking for in vitro validation of apoptosis and autophagy of schisandrin A on SCF/c-kit and TRPV1

The protein crystal structure files of the c-kit and TRPV1 were downloaded from Protein Data Bank (PDB). The crystal structure with higher resolution and corresponding bioactive ligands is preferred. The clean protein tool in Discovery Studio 2.5 (DS 2.5, Accelrys Inc., CA, USA) was used to prepare the protein, including deletion of the ligand, water molecules, and redundant protein conformation, completing incomplete residues, hydrogenating, and allocating related charges.

After the original ligand is taken out, it is redocked into the active pocket. If the root means square deviation (RMSD) is less than or equal to 2, it means that the related parameters can simulate the binding mode of the ligand and the protein, which could be used as the active pocket for further binding tests. Operation analysis tool was used to process docking results. Libdockscore was calculated to evaluate the best docking pose.

2.7. Western blotting and real-time PCR (RT-PCR) for further investigation of apoptosis and autophagy of schisandrin A on SCF/c-kit and TRPV1

0.5 mL radio-immunoprecipitation assay (RIPA) lysate containing protease inhibitor was added to 100 mg vibrated testicular tissue or 1×10^5 cells. The mixture was centrifuged (4 °C, 12,000 rpm, 15 min) to obtain the protein supernatant. The protein concentration was determined using commercial bicinchoninic acid assay (BCA) kits and then diluted to 10 μg/μL. The protein was isolated by 12% sodium dodecyl sulfate polyacrylamide gel electrophoresis (SDS-PAGE) electrophoresis and transferred to polyvinylidene difluoride (PVDF) membrane, blocked with skim milk for 2 h, and reacted with GAPDH antibody (Sungene Biotech, Tianjin, China) at 4 °C overnight, then goat anti-mouse & goat anti-rabbit antibodies (Jackson ImmunoResearch, PA, USA) for 1 h. After incubated with ECL colorant solution for 30 s, a digital gel image analysis system was used to take pictures and Image J software was used to calculate the gray value.

Total RNA was extracted from the testicular tissues of rats in each group, and the RNA quality was confirmed by spectrophotometry and agarose gel electrophoresis methods. DNA was removed from the RNA samples, and cDNA was generated by reverse transcription. PCR instrument was used for amplification, and RT-PCR reaction was conducted with a program of 95 °C pre-degeneration for 5 min, 95 °C for 15 s then 60 °C for 30 s for 40 cycles. Primers are shown in Supporting Information Table S2.

2.8. Statistical analysis

The results were expressed as mean ± SD. Statistical analyses were performed using SPSS13.0 (SPSS Inc., Chicago, IL, USA). One-way analysis of variance (ANOVA) followed by Dunnett's multiple comparison tests was used to compare differences among groups of samples. One-way ANOVA followed by student's t-test was used to evaluate biosensor performance. $P < 0.05$ was considered statistical significance, and $P < 0.01$ denoted very significant. Data analysis was performed on SPSS 20 (IBM, USA), SIMCA 14.1 (Umetrics, Sweden), and MATLAB R2016a (American Math Works).

3. Results and discussion

3.1. Superior efficacy of schisandrin A on testicular interstitial cells, sperm quality, and testicular tissue

3.1.1. Superior efficacy of schisandrin A on sperm quality and testicular tissue

Critical quality attribute (CQA) is a physical, chemical, biological, or microbiological property or characteristic that should be within an appropriate limit, range, and/or distribution to ensure desired product quality. CQAs proposed by the US Food and Drug Administration are generally associated with drug substances, excipients, intermediates (in-process materials), and drug products. Previous research has shown that schisandrin A is an essential and effective CQA of Huangjing Zanyu Capsules using serum medicinal chemistry analysis[13] (Supporting Information Fig. S1 and Table S3).

The effects of schisandrin A on model animals are shown in Fig. 1. Fig. 1A shows the pathological analysis of testicular tissues of five groups: normal, control (GTW), levocarnitine, Huangjing Zanyu Capsules (HJZY), and schisandrin A. In the section photos shown in Fig. 1A, spermatogonia cells were arranged in a regular order, with a large number and good structure (Fig. 1A (a4) (a5) (a9), and (a10)), which improved significantly compared with the model group (Fig. 1 (a2) and (a7)). Supporting Information Table S4 shows lesion grading and average scores. The above pathological analysis of testicular tissues indicates that schisandrin A significantly improved testicular lesions in model animals.

3.1.2. Superior efficacy of schisandrin A on testicular interstitial cells

Fig. 1C showed the effect of schisandrin A sperm quality. Fig. 1B (b1) shows the superior efficacy of schisandrin A on testicular interstitial cells. Schisandrin A of 10−40 μmol/L promoted proliferation of testicular interstitial cells, with the best effect observed at 10 μmol/L. Based on this, we believe that schisandrin A plays an important role in the regulation of reproductive function. Therefore, in-depth animal model experiments were conducted to clarify its action *in vivo*. The number of grades A nearly doubled after the intervention with a medium dose of schisandrin A (WWZ-M) (Fig. 1B (b2)). From Fig. 1B (b3), the proportion of grade B sperm increased from 8.52% to 12.51%. In addition, schisandrin A significantly improved the sperm density from 31.239% to 66.713% (Fig. 1B (b4)). Sperm motility (Fig. 1B (b5)) and viability (Fig. 1B (b6)) were also significantly improved and nearly tripled. Interestingly, schisandrin A from Huangjing Zanyu Capsules was more effective than the Huangjing Zanyu Capsules. In addition, the efficacy of schisandrin A was better than that of commercial L-carnitine.

In summary, schisandrin A demonstrated a positive effect on the recovery of diseased testicular tissue, ensuring the production of more high-quality sperm and easing the symptoms of oligoasthenospermia. Moreover, the above results indicate that the main focus should be on sperm density, grade A sperm, sperm motility, and viability between schisandrin A and oligoasthenospermia. These biological processes are inseparable from autophagy and apoptosis.

3.2. Fabrication and performance of SCF/c-kit biosensors

To elucidate the mechanism of schisandrin A in the treatment of oligoasthenospermia, the SCF/c-kit system was introduced, because it is an independent pathway related to the apoptosis of

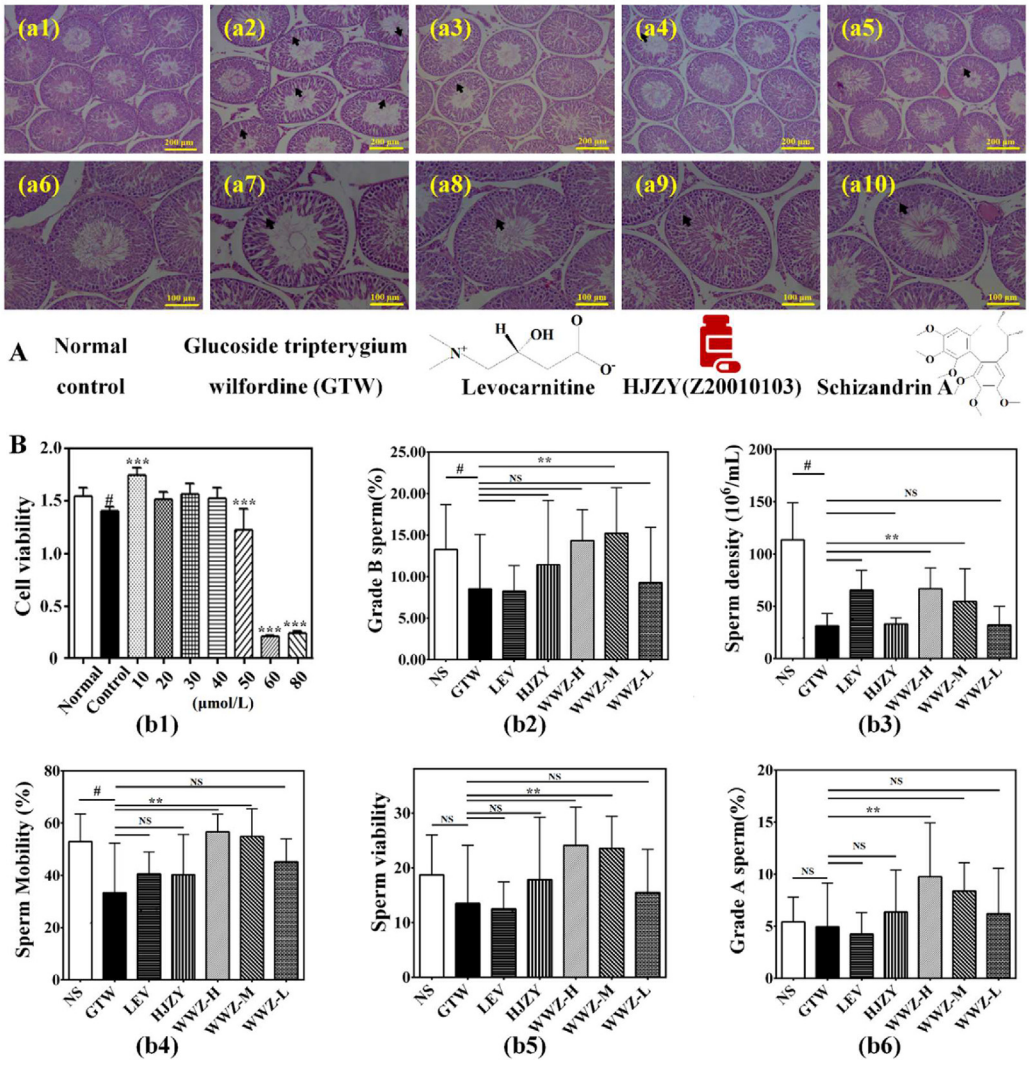

Figure 1 Superior efficacy of schisandrin A (CQA) on oligoasthenospermia. (A) Pathological sections of rat testis in each group magnified 200 and 400 times, respectively (black arrows pointed to the representative physiological and pathological characteristics). (a1) and (a6), Normal group; (a2) and (a7), model group by GTW; (a3) and (a8), group of levocarnitine; (a4) and (a9), group of Huangjing Zanyu capsule; (a5) and (a10), group of schisandrin A. (B) Superior efficacy of schisandrin A on testicular interstitial cells, sperm quality. (b1) Cell viability; (b2) grade A sperm (%); (b3) grade B sperm (%); (b4) sperm density; (b5) sperm mobility (%); (b6) sperm viability. Note: $^{\#}P < 0.05$ (*vs* normal group); $^{*}P < 0.05$, $^{**}P < 0.01$, $^{***}P < 0.001$ (*vs* control group).

spermatogenic cells in oligoasthenospermia. Therefore, a novel AlGaAs/GaAs HEMT device was developed and applied to the fabrication of SCF/c-kit biosensors[54] (Fig. 2A). Scanning electron microscopy (SEM) was used to reveal the surface microstructure of the AlGaAs/GaAs HEMT functionalized with SCF and c-kit. Fig. 2B shows the microstructure of the self-assembled monolayer and biosensor. After protein modification, several substances were visibly distributed on the chip compared to the smooth wafer of the uncovered chip. The percentages of C, N, and O are shown in Supporting Information Table S5. The percentage of the C, N, and O elements gradually increased with the fabrication of the protein on the chip, especially for c-kit. After c-kit protein modification, the C content increased from 16.4% to 23.8%, the O element from 5.1% to 15.8%, and the N element from 2.2% to 12.8%, respectively. These shifts were caused by the protein, which mainly consisted of C, N, and O. In addition, Fig. 2B (b3) shows a significant shift after the protein modification. These results indicated that the protein was successfully modified.

Furthermore, the perfect performance of the biosensors was characterized using the electrochemical workstation CHI660E, as summarized in Fig. 2C. Fig. 2C (c1) shows the I_{DS}-V_{DS} results for the 15 sampling intervals. There was little difference between the sampling intervals. Thus, given the efficiency and data processing, 0.05 s was determined as the best sampling interval. Similarly, a sampling interval of 0.1 V/s achieved a better speed (Fig. 2C (c2)). Given the stability of the biosensor, protein modification time was optimized. From the I_{DS}-V_{DS} and I_{DS}-T chat shown in Fig. 2C (c3) and (c4), it can be seen that after 2 h of protein modification, the biosensor reached a stable signal, and the signal did not change significantly. Similarly, after 4 min of sampling, the biosensor reached a relatively stable signal (Fig. 2C (c5)). Therefore, the modification time of the protein was determined to be 2 h and the reaction time of the sample was determined to be 4 min. Fig. 2C (c6) shows the reaction of samples with different concentrations with a blank chip. Gratifyingly, there was no change, and the RSD of the I_{DS}-V_{DS} curves was −1.275. Analysis of variance also

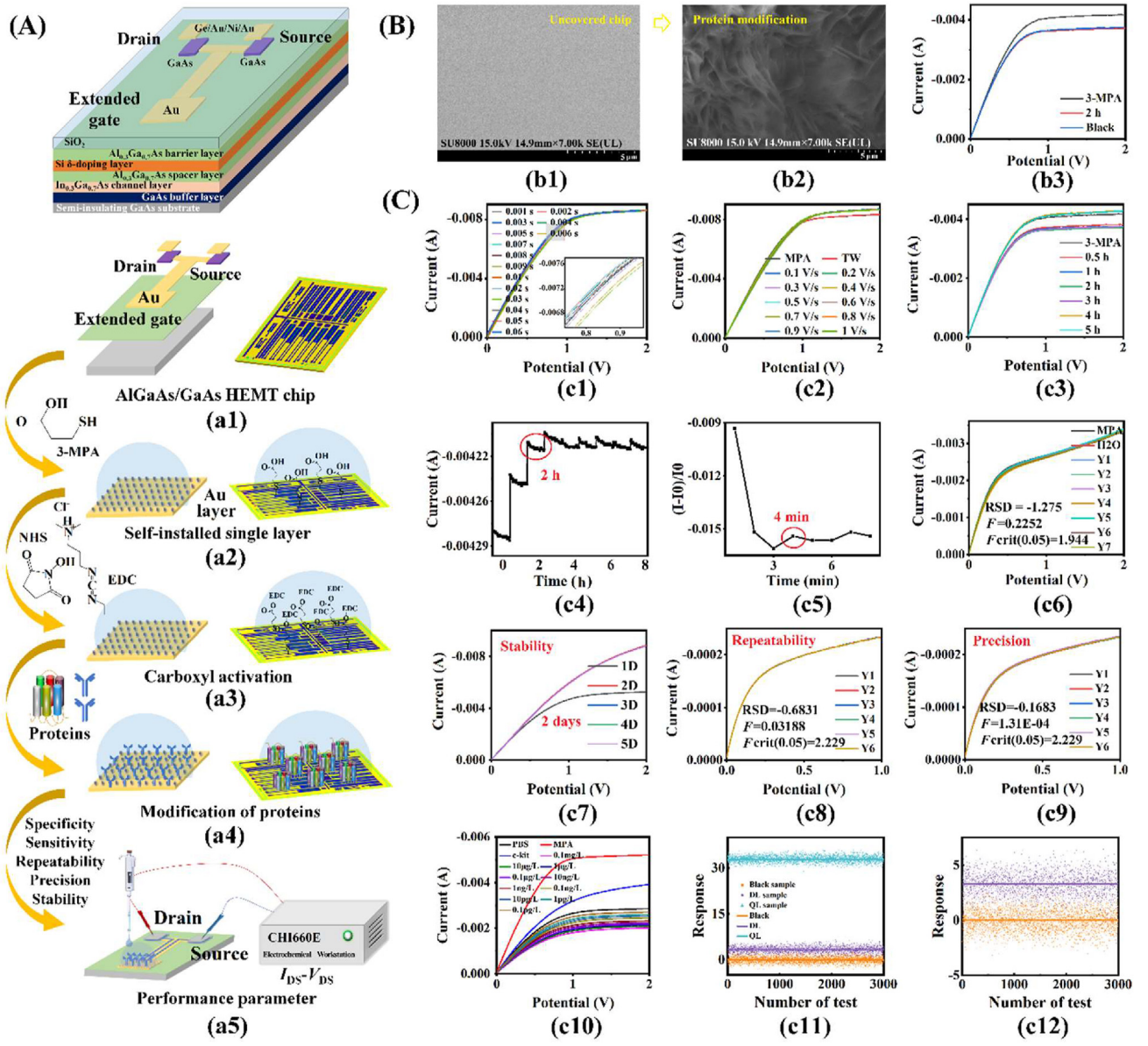

Figure 2 Fabrication and performance of SCF/c-kit biosensors. (A) The fabrication protocol of the new generation of SCF and c-kit biosensors. (B) The results of protein modification. (b1) SEM of Blank HEMT; (b2) SEM of HEMT modified protein; (b3) I_{DS}-V_{DS} shift caused by protein modification. (C) The parameter optimization and performance of c-kit biosensors. (c1) Sampling interval; (c2) scanning speed; (c3) protein modification time; (c4) and (c5) sample reaction time; (c6) specificity; (c7) stability; (c8) repeatability; (c9) precision; (c10) the I_{DS}-V_{DS} caused by tested samples with increasing concentration; (c11) and (c12) the simulated data of 3000 measurements for DL and QL.

showed that there was no difference between them ($F_{crit\ (0.05)}$ = 1.944). Additionally, BSA, as the negative control for biomacromolecules, barely interacted with c-kit (Supporting Information Fig. S2). Ferulic acid, as the negative control of natural small component, barely bound to c-kit (Supporting Information Fig. S3). Together, these findings confirm that biosensors can achieve strong specificity, which is the pivot of the biosensor. Fig. 2C (c7) shows the chip stability at 4 °C. It can be seen that the biosensors maintain good stability within 2 days and can completely meet the needs of detection. The results of six samples at the same concentration, which indicated good reproducibility of the biosensors, are shown in Fig. 2C (c8). The results of six repeated measurements of the same sample, which indicate perfect precision, are shown in Fig. 2C (c9). Interestingly, the repeatability and precision of the biosensor were excellent, with an RSD <0.7, marking a transcendental breakthrough in the mechanistic exploration of small molecules in complex biological processes.

In addition, based on the false negative error (recorded as α) and false positive error (recorded as β) theories, the detection limit (DL) and quantitation limit (QL) of the HEMT biosensor were defined as follows: Fig. 2C (c10) shows the response of I_{DS}-V_{DS} caused by the tested samples with increasing concentrations. Fig. 2C (c11) and (c12) show the simulated data of 3000 measurements for DL and QL. The response mean value of the blank control was x_0, and the variance was σ. The 90% confidence interval of the DL response value (recorded as x_1) was

$x_1-1.645\sigma - x_1+1.645\sigma$. Based on two types of error theories ($\alpha = 0.05$, $\beta = 0.05$), the response value of DL was $x_1 = x_0+3.29\sigma$. Correspondingly, the 95% confidence interval of QL (recorded as x_2) was $x_2-1.96\sigma$ to $x_2+1.96\sigma$. The QL response value $x_2 = x_{min}+3.92\sigma$. According to the Fig. 2C (c9), the response value of the black sample was −0.00281 A, and x_{min} was 1.0×10^{-13} mol/L. Therefore, DL was calculated as 2.787×10^{-15} mol/L, and QL was calculated as 1.0×10^{-13} mol/L.

In summary, original HEMT biosensors were successfully constructed. By extending the gated channel, the DL reached 2.787×10^{-15} g/L and the QL reached 1.0×10^{-13} g/L. In addition, it achieved a cut-off value of SCF and c-kit low of 0.1 pg/L, while the cut-off values of the commercial kits for SCF and c-kit were all around 10 pg/mL[64]. This is mainly attributed to the high sensitivity of two-dimensional electronic. Highly sensitive two-dimensional electron gases can convert signals for interactions between the substance to be measured and biological macromolecules without requiring additional labels, thus avoiding damage to protein activity. Furthermore, compared with classical HEMT chips, the HEMT used in this study was an extended-gate HEMT chip. The modification area was increased, so that the quantitative range of concentration greatly increased from 2 to 3 orders of magnitude to five orders of magnitude (0.1 pg/L to 1.0 ng/L). This was a significant innovation and improvement in the cutoff value and quantitative detection range.

3.3. Discovery of apoptosis mechanism of schisandrin A on SCF/c-kit system by HEMT biosensors coupled with in vitro and in vivo further investigation

3.3.1. Discovery of apoptosis mechanism of schisandrin A on SCF/c-kit system by HEMT biosensors

3.3.1.1. The interaction between SCF and c-kit. Based on previous biosensors and clinical samples[54], Fig. 3A shows the protocol for the measurement of SCF and c-kit biosensors. The shift in I_{DS}-V_{DS} between SCF and c-kit was detected and generalized in Fig. 3B (a1). There was clear a correlation between this shift and concentration, which suggested that there was a concentration-dependent interaction between SCF and c-kit, causing the shift of the two-dimensional electron gas in the HEMT devices, which changed the current between the source and drain. It is worth mentioning that SCF was detected at a concentration of only 0.1 pg/L. Furthermore, the logarithmically processed data could clearly show that the shift of I_{DS}-V_{DS} was linearly related to the logarithm of the concentration, especially in the range of 0.1 pg/L to 0.1 mg/L (Fig. 3B (a2)). According to Eq. (3), the K_D between SCF and c-kit was calculated to be $K_D = 3.686 \times 10^{-12}$ pg/L.

3.3.1.2. The interaction between schisandrin A and c-kit or SCF. Based on the aforementioned method, the I_{DS}-V_{DS} curve of the interaction between schisandrin A c-kit is shown in Fig. 3B (b1). It could be seen that the c-kit was immobilized on the HEMT surface and there was also a concentration dependent interaction between schisandrin A and c-kit. Furthermore, the logarithmically processed data showed a good linear correlation between the shift of I_{DS}-V_{DS} and the logarithm of the concentration, especially in the range of 0.1 pmol/L to 1 nmol/L (Fig. 3B (a2)). According to the linear fitting relationship between schisandrin A and c-kit, there was a strong interaction between schisandrin A and c-kit with a K_D of 5.701×10^{-11} mol/L. The same method was used to explore the interaction between schisandrin A and SCF using the SCF HEMT biosensor. Notably, the result was negative, and there was no interaction between schisandrin A and SCF.

3.3.1.3. The influence of schisandrin A on the interaction between SCF and c-kit. There was a strong interaction between SCF and c-kit, such as with schisandrin A and c-kit. However, there was no interaction between schisandrin A and SCF. The effect of schisandrin A on the SCF/c-kit system aroused interest. To explore this, the interaction between c-kit and the SCF and schisandrin A complex was investigated using a c-kit biosensor. Fig. 3B (c1−c3) exhibited the influence of different concentrations of SCF on the interaction between SCF and c-kit in the presence of the same concentration of schisandra A. Among them (c1) is a series of curves of I_{DS}-V_{DS} with increasing concentration of the above mixture (c2) is the linear fitting between the Lg of the above mixture concentration and $\Delta I/I_0$ (c3) is the linear fitting between the concentration/ΔI and the concentration of the above mixture. According to the Eqs. (1)−(3), K_D was calculated to be 1.026×10^{-10} mol/L. Simultaneously, the interaction between c-kit and the mixture consisting of the same concentration of SCF with different concentrations of schisandra A was further investigated, and similar results are shown in Fig. 3B (d1−d3). Likewise, K_D was calculated to be 1.357×10^{-10} mol/L. Compared with the K_D of pure SCF and c-kit (3.686×10^{-12} mol/L), the K_D between the mixture and c-kit decreased, which demonstrated that schisandrin A could interact well with c-kit when the amount of SCF was insufficient.

Collectively, it was surprisingly discovered that schisandrin A demonstrated tenacious affinity for c-kit, which was stronger than that of SCF. SCF can induce stem cells to enter the cell cycle, which not only promotes stem cell division but also inhibits apoptosis *in vivo*. The SCF/c-kit system plays a significant role in apoptosis, especially in testicular tissue. Therefore, we put forward a hypothesis that schisandrin A exerts an anti-apoptotic effect through the SCF/c-kit system. In support of our hypothesis, *in vitro* and *in vivo* validations were performed.

3.3.2. In vitro investigation of apoptosis mechanism of schisandrin A on SCF/c-kit system using molecular docking

Furthermore, Supporting Information Fig. S4 shows the molecular docking results of schisandrin A c-kit. It could be seen that hydrogen bonds could play a significant role in ligand binding. Hydrophobic bonds were mainly located in the nucleus of flavone. Compared with hydrogen bonds, hydrophobic interactions were more possibly involved in the binding process between schisandrin A and c-kit. One of the phenolic OH moieties and the vicinal carbonyl oxygen formed hydrogen bonds with the H atom of residue c-kit. These results indicated that there was indeed an interaction between schisandrin A c-kit.

3.3.3. In vivo investigation of apoptosis mechanism of schisandrin A on SCF/c-kit system by Western blot and RT-PCR

Moreover, Fig. 4A exhibited the TdT-mediated dUTP nick end labeling (TUNEL) assay results of testicular tissue samples in five groups, normal control, GTW, and different concentrations of schisandrin A. We found that GTW modeling caused an increase in the level of apoptosis in testicular tissue (Fig. 4A (a2), (a7), and (a12)), which was reversed by schisandrin A (Fig. 4A (a3)−(a5), (a8)−(a10), (a13)−(a15)). Simultaneously, Western blotting and real-time PCR (RT-PCR) were used to validate this hypothesis, and

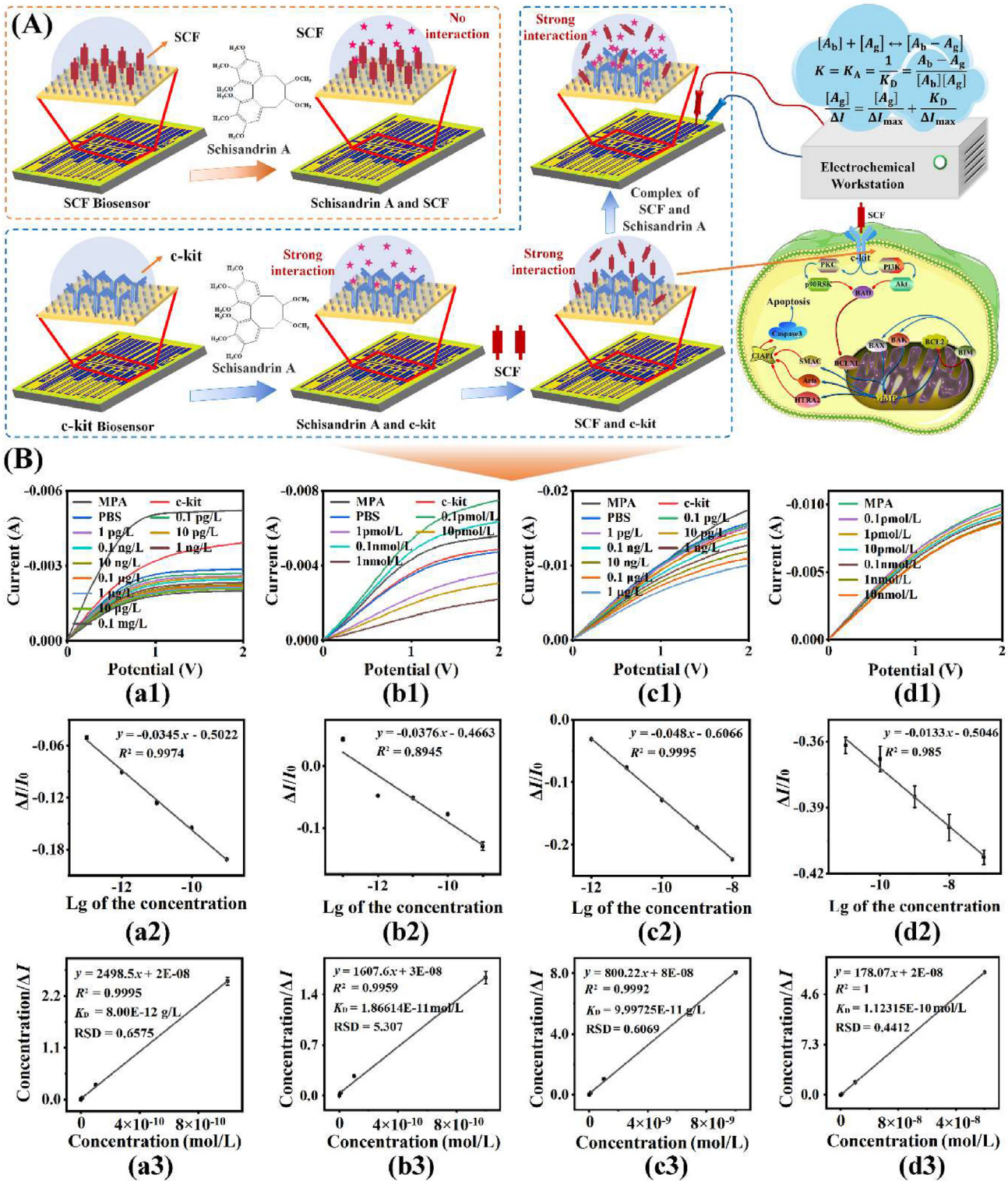

Figure 3 Discovery of apoptosis mechanism of schisandrin A on SCF/c-kit system. (A) Schematic diagram of interaction results between schisandrin A and SCF/c-kit biosensors. (B) Interaction results between schisandrin A and SCF/c-kit biosensors by CHI660E and artificial intelligence algorithm. (a1)−(d1) I_{DS}-V_{DS} decreases (ΔI) with increasing concentration (record as C) of SCF, schisandrin A, the complex of SCF added schisandrin A, the complex of schisandrin A added SCF; (a2)−(d2) The linear fitting between Lg of C and $\Delta I/I_0$ of SCF added schisandrin A, the complex of schisandrin A added SCF; (a3)−(d3) $C/\Delta I$ *versus* C of SCF added schisandrin A, the complex of schisandrin A added SCF.

the results of each group are shown in Fig. 4B. In favor of our ratiocination, through the intervention of a high dose of schisandrin A (WWZ-H group), the expression of c-kit protein was nearly double that of the model group (Fig. 4B (b1)). Compared with the results of gene expression levels of c-kit in each group, as shown in Fig. 4B (b2), it can be seen that the expression level of SCF was increased in the oligoasthenospermia model group, whereas the middle dosage group of schisandrin A decreased the expression level. In addition, the gene expression level of SCF protein also showed a significant upward trend in the schisandrin A group (Fig. 4B (b3)), but this trend was contrary to the expression level of its gene (Fig. 4B (b4)). This indicated that both protein expression and gene expression of SCF were reduced in the oligoasthenospermia model group, resulting in a lower amount of the SCF/c-kit system *in vivo* and consequently reduced sperm production.

Additionally, Fig. 4C (c1) and (c2) display the schematic diagrams of oligoasthenia and asthenospermia. Combined with the results of the SCF/c-kit biosensors, it can be seen that schisandrin A interact with c-kit. Notably, the schisandrin A demonstrated tenacious affinity for c-kit, which was stronger than that of SCF. Compared to the normal group, the model group had a higher level of c-kit, which may be due to the lack of SCF. Fig. 4C (c3) shows a schematic representation of schisandrin A-modulated oligoasthenospermia. Firstly, excess c-kit on germ cells was occupied by schisandrin A, after taking schisandrin A. Then, the schisandrin A/c-kit system which was similar to the SCF/c-kit system was activated, improving the proliferation and differentiation of germ cells. Furthermore, as shown in Fig. 4C (c4), FSH secreted by germ cells increased, which was critical for the differentiation of Sertoli cells to secrete SCF. In this way, the balance between SCF and c-kit can be restored to maintain normal differentiation and apoptosis of germ cells.

Overall, schisandrin A can regulate cell apoptosis through the SCF/c-kit system. Thus, the above data validate the results of biosensors that schisandrin A indeed exerted therapeutic effects on oligoasthenospermia by acting on the SCF/c-kit system, which regulates the related pathways of apoptosis, as shown in the diagram of anti-apoptotic pathways in Fig. 3A section.

3.4. Discovery of the essential role of schisandra A on the interplay between autophagy and apoptosis in oligoasthenospermia

3.4.1. Discovery of the essential role of schisandra A on autophagy mechanism in oligoasthenospermia by TRPV1 biosensor

The above results unambiguously demonstrated that schisandrin A exerted an anti-apoptotic effect through SCF/c-kit to restore the spermatogenesis ability of oligoasthenospermia. However, autophagy and apoptosis often occur in the same cell type, in which autophagy precedes apoptosis[65]. In many cases, if the cell commences apoptosis, autophagy can be inactivated[66]. Essential proteins involved in the autophagic process may promote cell death by catabolizing organelles or facilitating the activation of apoptotic[67,68]. Therefore, we introduced the TRPV1 biosensor to monitor the complex relationship between autophagy and apoptosis, focusing on the impact of intersecting signal transduction pathways on oligoasthenospermia.

Fig. 5A shows a schematic representation of the creation and monitoring of the TRPV1 biosensor. Firstly, Fig. 5B (b1) and (b2) show the microstructures of the self-assembled monolayer and the TRPV1 biosensor, respectively. As a result, after protein modification, more substances were distributed on the chip than on the uncovered chip. The changes in C, N, and O are summarized in Supporting Information Table S5. The visible percentages of C, N, and O gradually increased with the development of TRPV1. Specifically, the C content increased from 13.8% to 17%, the O content increased from 5.2% to 9.2%, and the N content increased from 7.5% to 18.5%. These shifts were caused by the protein, which mainly consisted of C, N, and O. These results demonstrated that the TRPV1 biosensor was successfully fabricated.

Furthermore, using the fabricated TRPV1 biosensor, the mechanism of action of schisandrin A autophagy in oligoasthenospermia was investigated. Fig. 5C (c1) shows the I_{DS}-V_{DS} results detected by differential pulse voltammetry (DPV) method. First, electrochemical signals illustrated that the current decreased owing to the resistance caused by the TRPV1 protein. Interestingly, the interaction between the TRPV1 biosensor and schisandrin A demonstrated a concentration-dependent relationship. The interaction between schisandrin A and TRPV1 with 11 concentration gradients covering the concentration range of 10^{10} mol/L was analyzed and is shown in Fig. 5C (c2) and (c3). It could be seen that this biosensor could detect schisandrin A of 0.1 pmol/L, while the quantitative concentration ranged from 1.0 pmol/L up to 0.01 mmol/L. The K_D was calculated to be 4.181×10^{-10} mol/L. This demonstrated that schisandrin A had a strong interaction with TRPV1. Therefore, we hypothesized that schisandrin A may affect autophagy and apoptosis in oligoasthenospermia through TRPV1.

3.4.2. In vivo investigation of schisandra A on the interplay between autophagy and apoptosis in oligoasthenospermia

Supporting Information Fig. S5 shows the molecular docking results for schisandrin A and TRPV1. It could be seen that hydrogen bond, Pi−alkyl, Unfavorable Bump, and van der Waals forces could play a significant role in ligand binding, which indicated that there was indeed interaction between schisandrin A and TRPV1.

3.4.3. In vivo investigation of schisandra A on the interplay between autophagy and apoptosis in oligoasthenospermia

Over and above that, in favor of our ratiocination, the expression of critical downstream proteins of TRPV1 during autophagy and apoptosis was detected. Fortunately, the expression of these critical proteins verified this conjecture (Fig. 5D). Schisandrin A reduced the level of Akt (Fig. 5D (d1)) but increased the level of phosphorylated Akt (p-Akt) (Fig. 5D (d2)). As shown in Fig. 5D (d3), the ratio of p-Akt to Akt was significantly elevated. The level of apoptosis was also increased by modeling. In terms of apoptosis-related proteins, Fig. 5D (d4) showed that the expression of Bcl-2 protein in each group of schisandrin A had an up-regulated trend, illustrating that administration could inhibit spermatocyte apoptosis. Upregulation of Bcl-2 promotes the formation of the heterodimer Bcl-2/Bax instead of the homodimer Bax/Bax, resulting in the reduction of spermatocyte apoptosis. In addition, Fig. 5D (d5) and (d6) show that schisandrin A slightly increased the level of MDM2 and decreased the level of p53.

Moreover, LC3B-II, which characterizes the level of autophagy, was highly expressed in the model group, indicating an excessive state of autophagy (Fig. 5D (d7) and (d8)). Thus, we speculated that spermatocytes undergo excessive autophagy after ACR modeling. There was a statistically significant difference in the high-dose schisandrin A group ($P < 0.01$). Simultaneously,

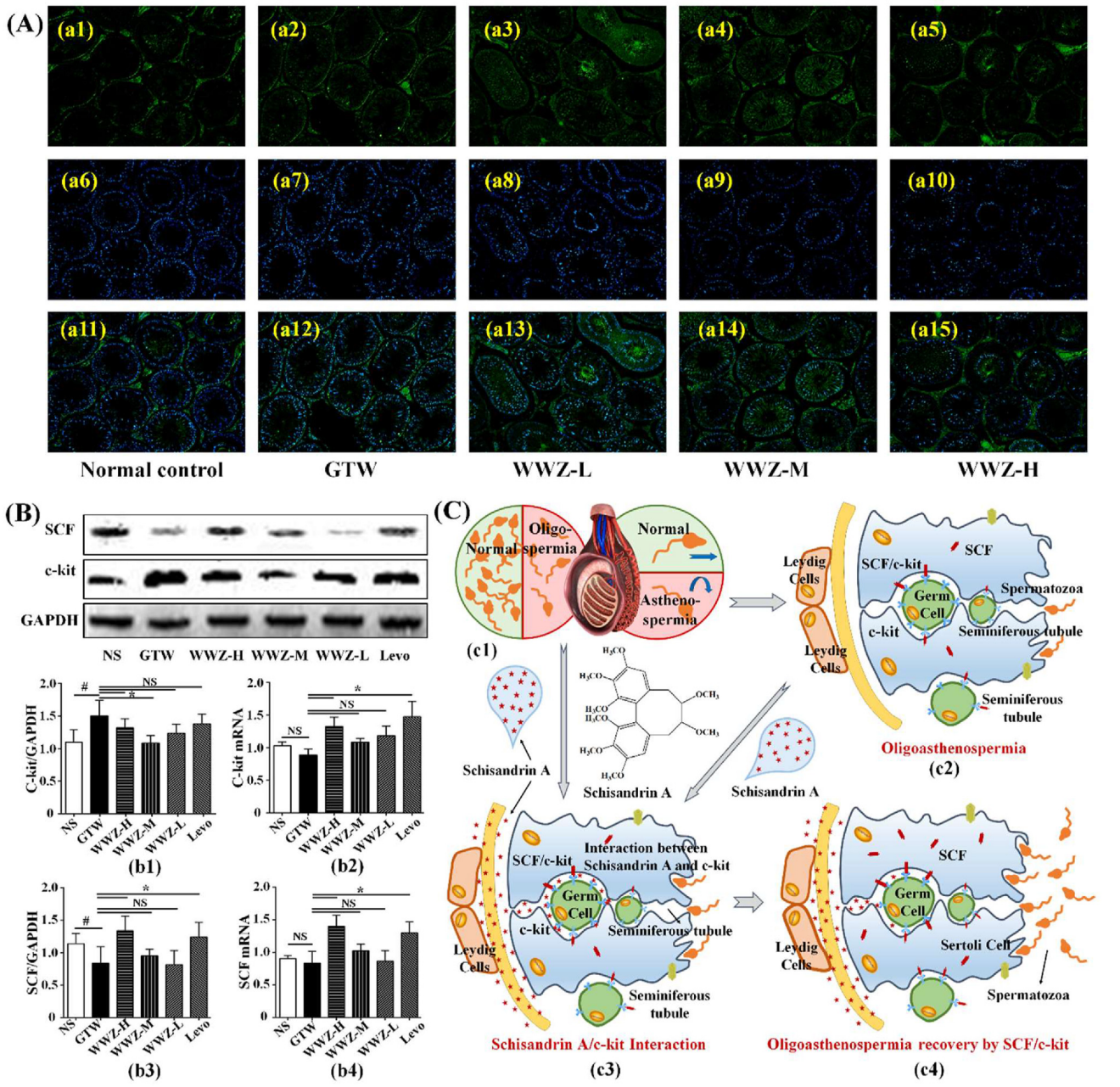

Figure 4 (A) TUNEL assay for testicular tissue samples in different groups. (a1)−(a5) The TUNEL assay results of normal control, GTW, WWZ-L, WWZ-M, and WWZ-H, respectively; (a6)−(a10) The DAPI results of normal control, GTW, WWZ-L, WWZ-M, and WWZ-H, respectively; (a11)−(a15) The merge charts by TUNEL and DAPI of normal control, GTW, WWZ-L, WWZ-M, and WWZ-H, respectively. (B) Western blot strip charts and RT-PCR results of SCF and c-kit expression in different groups. (b1) c-kit protein; (b2) c-kit mRNA; (b3) SCF protein; (b4) SCF mRNA. $^{*}P < 0.05$ *vs* NS group; $^{\#}P < 0.05$ *vs* GTW group in all figures. (C) The schematic diagram of oligoasthenospermia by schisandrin A. (c1) The schematic diagram of oligoasthenia; and (c2) The schematic diagram of asthenospermia; (c3) The schematic representation of schisandrin A modulated oligoasthenospermia; (c4) The schematic diagram of oligoasthenospermia recovery by SCF/c-kit system.

the levels of Beclin-1, ULK1, and p-ULK1 were investigated, and are summarized in Fig. 5D (d9)−(d12). As a result, p-ULK1/ULK1 increased in the schisandrin A group, which indicates that schisandrin A may reduce excessive autophagy and reduce the damage of ACR to spermatocytes through the ULK1/mechanistic target of rapamycin (mTOR) pathway (Fig. 5E). The results of autophagy-related modeling were shown in the Supporting Information Figs. S6 and S7.

In short, after the action of schisandrin A, which targets TRPV1 and the SCF/c-kit system, the level of p-Akt increased *in vivo*, leading to a decrease in the level of MDM2, which inhibits p53 production. This results in the reduction of caspase-3, which inhibits apoptosis. The interaction of schisandrin A with TRPV1 and the SCF/c-kit system could simultaneously increase p-Akt/Akt and consequently promote mTOR production, which leads to increased levels of p-ULK1/ULK1 and reduces excessive

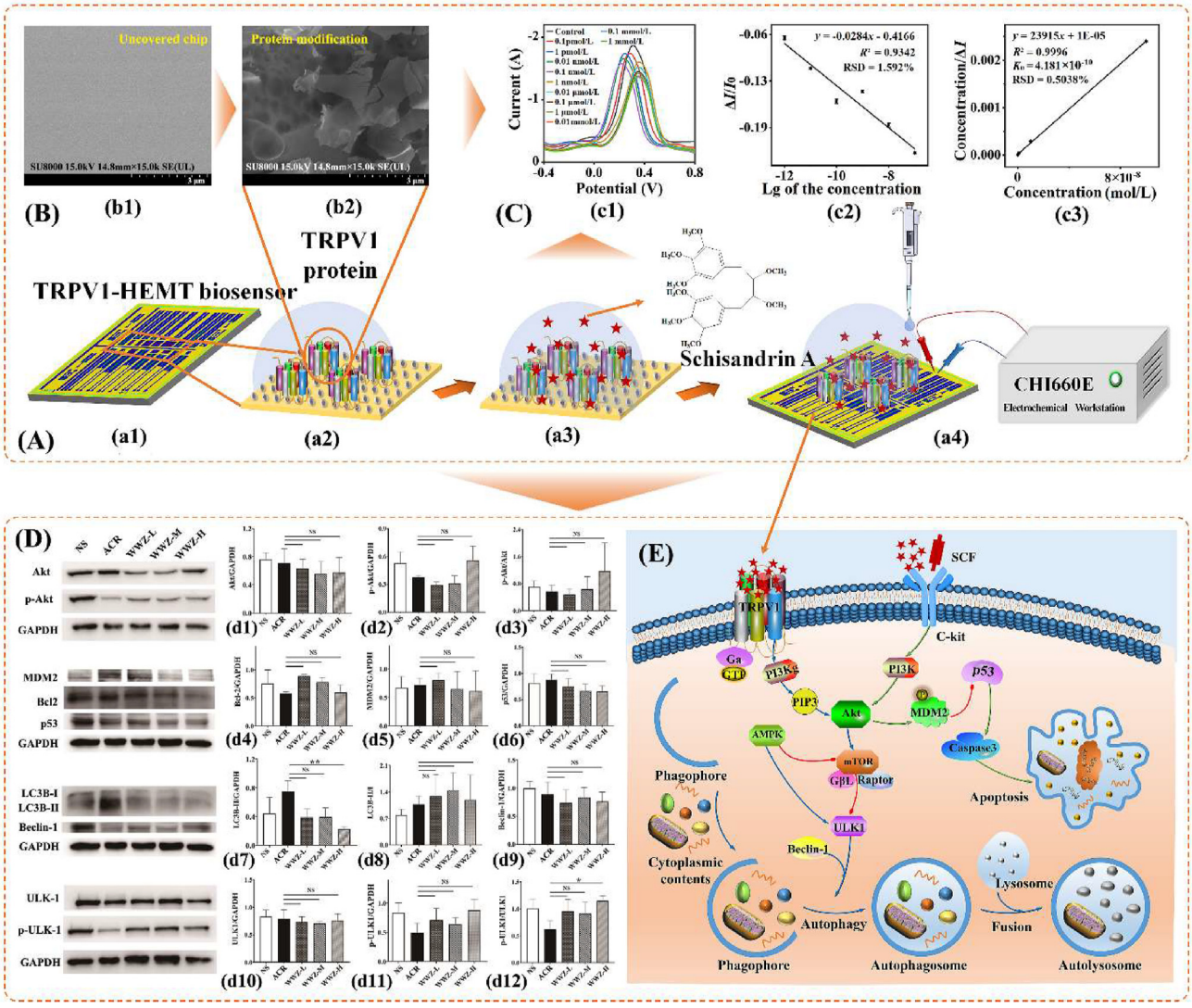

Figure 5 The interplay between autophagy and apoptosis in oligoasthenospermia by schisandra A. (A) Schematic diagram of interaction between schisandrin A and TRPV1 biosensor. (a1) The TRPV1-HEMT biosensor; (a2) The enlarged view of the protein modified area; (a3) The interaction between schisandrin A and TRPV1-HEMT biosensor; (a4) The detection of interaction between schisandrin A and TRPV1 by CHI660E. (B) The results of protein modification. (b1) SEM of blank HEMT (b2) SEM of HEMT modified protein. (C) Interaction results between schisandrin A and TRPV1 by CHI660E and artificial intelligence algorithm. (c1) I_{DS}-V_{DS} regularity decreases with increasing concentration of schisandrin A; (c2) The linear fitting between Lg of schisandrin A concentration and $(I-I_0)/I_0$; (c3) $[A_g]/\Delta I$ *versus* $[A_g]$ of schisandrin A. (D) Western blot strip charts and expression levels of autophagy- and apoptosis-related proteins. (d1) Akt; (d2) p-Akt; (d3) p-Akt/Akt; (d4) Bcl-2; (d5) MDM2; (d6) p53; (d7) LC3B-II; (d8) LC3B-II/I; (d9) Beclin1; (d10) ULK1; (d11) p-ULK1; (d12) p-ULK1/ULK1. Note: $^*P < 0.05$, $^{**}P < 0.01$ (E) The schematic diagram of schisandrin A regulating the interplay of autophagy and apoptosis through TRPV1 and SCF/c-kit systems.

autophagy. This indicated that the regulatory effect of schisandrin A on spermatocyte autophagy and apoptosis for the recovery of oligoasthenospermia included the recovery of diseased testicular tissue, ensuring the production of more high-quality sperm, and easing the symptoms. Furthermore, c-kit and TRPV1 may be two vital potential targets of schisandrin A in curing oligoasthenospermia.

In summary, based on their excellent performance, these biosensors were adopted and successfully achieved the interplay between apoptosis and autophagy to identify potential targets and effective candidates for oligoasthenospermia. This blazed new trails for interaction mechanism studies based on biosensors and avoided the limitations of unilateral studies, compared with existing unilateral studies of autophagy or apoptosis, which marked a transcendental breakthrough for the mechanistic exploration of small molecules in complex biological processes.

4. Conclusions

In this study, three highly sensitive and specific extended-gate HEMT biosensors were successfully developed and applied to the investigation of the interplay between apoptosis and autophagy. By extending the gated channel, the DL of the biosensor reached 2.787×10^{-15} g/L, QL reached 1.0×10^{-13} g/L, the quantitative range was increased from 2 to 3 orders of magnitude to five orders

of magnitude (0.1 pg/L to 1.0 ng/L) compared with existing biosensors. This was a significant innovation and improvement in the cutoff value and quantitative detection range. Based on this, we determined the interplay between apoptosis and autophagy in oligoasthenospermia and successfully identified effective candidates and potential targets for the first time, marking a transcendental breakthrough in the strategy for mechanistic exploration of small molecules in complex biological processes. Future studies will focus on developing an original biosensor array modified by multiple receptors to angle CQAs with efficacy in CMM.

Acknowledgments

This work was co-supported by National Outstanding Youth Science Fund Project of National Natural Science Foundation of China (No. 82022073), National Natural Science Foundation of China (No. 82174389), Natural Science Foundation of Beijing Municipality (No. 7202115, China), and Postdoctoral Research Foundation of China (No. 2021M690474). We thank Shenzhen Crystalo Biopharmaceutical Co., Ltd. (Shenzhen, China) for TRPV1 protein purification.

Author contributions

Lijuan Ma: Experiment, Data curation, Formal analysis, Software, Writing-original draft, Writing-review&editing, Visualization, Validation. Boyi Li: Experiment, Data curation, Software. Jinchen Ma: Writing-original draft, Validation. Chunyuan Wu: real-word products and samples supplying. Nan Li: Visualization. Kailin Zhou: Visualization. Yun Yan: Experiment. Mingshuang Li: Visualization. Xiaoyan Hu: Visualization. Hao Yan: Visualization. Qi Wang: Conceptualization, Supervision. Yanfei Zheng: Conceptualization, Supervision. Zhisheng Wu: Conceptualization, Funding acquisition, Project administration, Supervision.

Conflicts of interest

The authors declare no competing interests.

Appendix A. Supporting information

Supporting data to this article can be found online at https://doi.org/10.1016/j.apsb.2023.01.004.

References

1. Minhas S, Bettocchi C, Boeri L, Capogrosso P, Carvalho J, Cilesiz NC, et al. European association of urology guidelines on male sexual and reproductive health: 2021 update on male infertility. *Eur Urol* 2021;**80**:603−20.
2. Cooper TG, Noonan E, von Eckardstein S, Auger J, Baker HW, Behre HM, et al. World health organization reference values for human semen characteristics. *Hum Reprod Update* 2010;**16**:231−45.
3. Hammoud AO, Gibson M, Peterson CM, Meikle AW, Carrell DT. Impact of male obesity on infertility: a critical review of the current literature. *Fertil Steril* 2008;**90**:897−904.
4. Rowe PJ, World Health Organization. *WHO manual for the standardized investigation, diagnosis, and management of the infertile male*. New York: Cambridge University Press; 2000.
5. Jungwirth A, Giwercman A, Tournaye H, Diemer T, Kopa Z, Dohle G, et al. European association of urology guidelines on male infertility: the 2012 update. *Eur Urol* 2012;**62**:324−32.
6. Tvrda E, Agarwal A, Alkuhaimi N. Male reproductive cancers and infertility: a mutual relationship. *Int J Mol Sci* 2015;**16**:7230−60.
7. Sucher NJ. The application of Chinese medicine to novel drug discovery. *Expet Opin Drug Discov* 2013;**8**:21−34.
8. Lyu M, Fan GW, Xiao GX, Wang TY, Xu D, Gao J, et al. Traditional Chinese medicine in COVID-19. *Acta Pharm Sin B* 2021;**11**:3337−63.
9. Luo P, Liu DD, Zhang Q, Yang F, Wong YK, Xia F, et al. Celastrol induces ferroptosis in activated HSCs to ameliorate hepatic fibrosis *via* targeting peroxiredoxins and HO-1. *Acta Pharm Sin B* 2022;**12**:2300−14.
10. Guo ZR. Artemisinin anti-malarial drugs in China. *Acta Pharm Sin B* 2016;**6**:115−24.
11. Dolivo D, Weathers P, Dominko T. Artemisinin and artemisinin derivatives as anti-fibrotic therapeutics. *Acta Pharm Sin B* 2021;**11**:322−39.
12. Cao YH, Fang JH, Shi YW, Wang H, Chen XF, Liu Y, et al. Screening potential p-glycoprotein inhibitors by combination of a detergent-free membrane protein extraction with surface plasmon resonance biosensor. *Acta Pharm Sin B* 2022;**12**:3113−23.
13. Zheng Y. *The discovery of chemical components and mechanism of improving oligoasthenospermia of Huangjingzanyu capsule* [doctor]. Beijing University of Chinese Medicine; 2014.
14. Choi YH. Schisandrin a prevents oxidative stress-induced DNA damage and apoptosis by attenuating ROS generation in C2C12 cells. *Biomed Pharmacother* 2018;**106**:902−9.
15. Lu Y, Wang WJ, Song YZ, Liang ZQ. The protective mechanism of schisandrin a in D-galactosamine-induced acute liver injury through activation of autophagy. *Pharm Biol* 2014;**52**:1302−7.
16. Peter ME. Apoptosis meets necrosis. *Nature* 2011;**471**:310−2.
17. Fuchs Y. The therapeutic promise of apoptosis. *Science* 2019;**363**:1050−1.
18. Fuchs Y, Brown S, Gorenc T, Rodriguez J, Fuchs E, Steller H. Sept 4/ARTS regulates stem cell apoptosis and skin regeneration. *Science* 2013;**341**:286−9.
19. Gump JM, Thorburn A. Autophagy and apoptosis: what is the connection?. *Trends Cell Biol* 2011;**21**:387−92.
20. Lakhani SA, Masud A, Kuida K, Porter GA, Booth CJ, Mehal WZ, et al. Caspases 3 and 7: key mediators of mitochondrial events of apoptosis. *Science* 2006;**311**:847−51.
21. Sandlow JI, Feng HL, Cohen MB, Sandra A. Expression of c-kit and its ligand, stem cell factor, in normal and subfertile human testicular tissue. *J Androl* 1996;**17**:403−8.
22. Mruk DD, Cheng CY. Sertoli-sertoli and sertoli-germ cell interactions and their significance in germ cell movement in the seminiferous epithelium during spermatogenesis. *Endocr Rev* 2004;**25**:747−806.
23. Sato T, Yokonishi T, Komeya M, Katagiri K, Kubota Y, Matoba S, et al. From the cover: testis tissue explantation cures spermatogenic failure in c-kit ligand mutant mice. *Proc Natl Acad Sci U S A* 2012;**109**:16934−8.
24. Yan W, Suominen J, Toppari J. Stem cell factor protects germ cells from apoptosis *in vitro*. *J Cell Sci* 2000;**113**(Pt 1):161−8.
25. Correia S, Alves MR, Cavaco JE, Oliveira PF, Socorro S. Estrogenic regulation of testicular expression of stem cell factor and c-kit: implications in germ cell survival and male fertility. *Fertil Steril* 2014;**102**:299−306.
26. Ohta H, Yomogida K, Dohmae K, Nishimune Y. Regulation of proliferation and differentiation in spermatogonial stem cells: the role of C-kit and its ligand SCF. *Development* 2000;**127**:2125−31.
27. Blume-Jensen P, Claesson-Welsh L, Siegbahn A, Zsebo KM, Heldin CH. Activation of the human c-kit product by ligand-induced dimerization mediates circular actin reorganization and chemotaxis. *EMBO J* 1992;**10**:4121−8.
28. Figueira MI, Cardoso HJ, Correia S, Maia CJ, Socorro S. The stem cell factor (SCF)/c-kit system in carcinogenesis of reproductive tissues: what does the hormonal regulation tell us?. *Cancer Lett* 2017;**405**:10−21.
29. Levine B, Klionsky DJ. Development by self-digestion: molecular mechanisms and biological functions of autophagy. *Dev Cell* 2004;**6**:463−77.
30. Sorice M. Crosstalk of autophagy and apoptosis. *Cells* 2022;**11**:1479.

31. Eisenberg-Lerner A, Bialik S, Simon HU, Kimchi A. Life and death partners: apoptosis, autophagy and the cross-talk between them. *Cell Death Differ* 2009;**16**:966−75.
32. Sukumaran P, Nascimento Da Conceicao V, Sun Y, Ahamad N, Saraiva LR, Selvaraj S, et al. Calcium signaling regulates autophagy and apoptosis. *Cells* 2021;**10**:2125.
33. Sui XB, Kong N, Ye L, Han WD, Zhou JC, Zhang Q, et al. p38 and JNK MAPK pathways control the balance of apoptosis and autophagy in response to chemotherapeutic agents. *Cancer Lett* 2014;**344**:174−9.
34. Brunelli F, Torosantucci L, Gelmetti V, Franzone D, Grünewald A, Krüger R, et al. PINK1 protects against staurosporine-induced apoptosis by interacting with beclin 1 and impairing its pro-apoptotic cleavage. *Cells* 2022;**11**:678.
35. Ravegnini G, Sammarini G, Nannini M, Pantaleo MA, Biasco G, Hrelia P, et al. Gastrointestinal stromal tumors (GIST): facing cell death between autophagy and apoptosis. *Autophagy* 2017;**13**:452−63.
36. Smaili SS, Pereira GJS, Costa MM, Rocha KK, Rodrigues L, do Carmo LG, et al. The role of calcium stores in apoptosis and autophagy. *Curr Mol Med* 2013;**13**:252−65.
37. Voets T, Droogmans G, Wissenbach U, Janssens A, Flockerzi V, Nilius B. The principle of temperature-dependent gating in cold- and heat-sensitive TRP channels. *Nature* 2004;**430**:748−54.
38. Dai W, Bai Y, Hebda L, Zhong X, Liu J, Kao J, et al. Calcium deficiency-induced and TRP channel-regulated IGF1R-PI3K-Akt signaling regulates abnormal epithelial cell proliferation. *Cell Death Differ* 2014;**21**:568−81.
39. Nabissi M, Morelli MB, Amantini C, Liberati S, Santoni M, Ricci-Vitiani L, et al. Cannabidiol stimulates Aml-1a-dependent glial differentiation and inhibits glioma stem-like cells proliferation by inducing autophagy in a TRPV2-dependent manner. *Int J Cancer* 2015;**137**:1855−69.
40. Yuan JX, Liu HH, Zhang H, Wang TT, Zheng Q, Li Z. Controlled activation of TRPV1 channels on microglia to boost their autophagy for clearance of alpha-synuclein and enhance therapy of Parkinson's disease. *Adv Mater* 2022;**34**:e2108435.
41. Huang TT, Lin Y, Pang QY, Shen WM, Chen X, Tu FX. The synergistic effect of TRPV1 on oxidative stress-induced autophagy and apoptosis in microglia. *Anal Cell Pathol* 2021;**2021**:7955791.
42. Amantini C, Farfariello V, Cardinali C, Morelli MB, Marinelli O, Nabissi M, et al. The TRPV1 ion channel regulates thymocyte differentiation by modulating autophagy and proteasome activity. *Oncotarget* 2017;**8**:90766−80.
43. Klionsky DJ, Cuervo AM, Seglen PO. Methods for monitoring autophagy from yeast to human. *Autophagy* 2007;**3**:181−206.
44. Fleming A, Bourdenx M, Fujimaki M, Karabiyik C, Krause GJ, Lopez A, et al. The different autophagy degradation pathways and neurodegeneration. *Neuron* 2022;**110**:935−66.
45. Li W, He P, Huang Y, Li YF, Lu J, Li M, et al. Selective autophagy of intracellular organelles: recent research advances. *Theranostics* 2021;**11**:222−56.
46. Yim WWY, Mizushima N. Lysosome biology in autophagy. *Cell Discovery* 2020;**6**:6.
47. Rosado CJ, Mijaljica D, Hatzinisiriou I, Prescott M, Devenish RJ. Rosella−a fluorescent pH-biosensor for reporting vacuolar turnover of cytosol and organelles in yeast. *Autophagy* 2008;**4**:205−13.
48. Zhai SY, Hu W, Wang WB, Chai L, An Q, Li CY, et al. Tracking autophagy process with a through bond energy transfer-based ratiometric two-photon viscosity probe. *Biosens Bioelectron* 2022;**213**:114484.
49. Mao SF, Li WW, Zhang Q, Zhang WL, Huang QS, Lin JM. Cell analysis on chip-mass spectrometry. *Trac-Trend Anal Chem* 2018;**107**:43−59.
50. Wu J, Chen QS, Liu W, Zhang YD, Lin JM. Cytotoxicity of quantum dots assay on a microfluidic 3D-culture device based on modeling diffusion process between blood vessels and tissues. *Lab Chip* 2012;**12**:3474−80.
51. Espinosa N, Schwarz SU, Cimalla V, Ambacher O. Detection of different target-DNA concentrations with highly sensitive AlGaN/GaN high electron mobility transistors. *Sensor Actuat B-Chem* 2015;**210**:633−9.
52. Chen YW, Tai TY, Hsu CP, Sarangadharan I, Pulikkathodi AK, Wang HL, et al. Direct detection of DNA using electrical double layer gated high electron mobility transistor in high ionic strength solution with high sensitivity and specificity. *Sensor Actuat B-Chem* 2018;**271**:110−7.
53. Li C, Curreli M, Lin H, Lei B, Ishikawa FN, Datar R, et al. Complementary detection of prostate-specific antigen using In_2O_3 nanowires and carbon nanotubes. *J Am Chem Soc* 2005;**127**:12484−5.
54. Ma LJ, Zheng YF, Wang J, Li QQ, Zeng JQ, Wang ZJ, et al. Development of MIF/IL-1 beta biosensors for discovery of critical quality attributes and potential allergic rhinitis targets from clinical real-world data by intelligent algorithm coupled with *in vitro* and *vivo* mechanism validation. *Biosens Bioelectron* 2021;**194**:113608.
55. Shen MY, Li BR, Li YK. Silicon nanowire field-effect-transistor based biosensors: from sensitive to ultra-sensitive. *Biosens Bioelectron* 2014;**60**:101−11.
56. Ma SW, Zhang XH, Liao QL, Liu HS, Huang YH, Song Y, et al. Enzymatic lactic acid sensing by In-doped ZnO nanowires functionalized AlGaAs/GaAs high electron mobility transistor. *Sensor Actuat B-Chem* 2015;**212**:41−6.
57. Guan SQ, Zhu YT, Wang JS, Dong L, Zhao Q, Wang L, et al. A combination of Semen Cuscutae and Fructus Lycii improves testicular cell proliferation and inhibits their apoptosis in rats with spermatogenic dysfunction by regulating the SCF/c-kit-PI3K-Bcl-2 pathway. *J Ethnopharmacol* 2020;**251**:112525.
58. Anderson D, Bishop JB, Garner RC, Ostrosky-Wegman P, Selby PB. Cyclophosphamide: review of its mutagenicity for an assessment of potential germ cell risks. *Mutat Res-Fund Mol M* 1995;**330**:115−81.
59. Khedr NF, Werida RH. L-Carnitine modulates autophagy, oxidative stress and inflammation in trazodone induced testicular toxicity. *Life Sci* 2022;**290**:120025.
60. Sigman M, Glass S, Campagnone J, Pryor JL. Carnitine for the treatment of idiopathic asthenospermia: a randomized, double-blind, placebo-controlled trial. *Fertil Steril* 2006;**85**:1409−14.
61. Li BY, Ma JC, Zhu LH, Yan Y, Wu YQ, Zheng CL, et al. Metabolomic profiling and alleviation of oxidative stress of Huangjing Zanyu capsule treating oligoasthenospermia. *Transl Androl Urol* 2022;**11**:659−74.
62. Wang CC, Chen HJ, Chan DC, Chiu CY, Liu SH, Lan KC. Low-Dose Acrolein, an endogenous and exogenous toxic molecule, inhibits glucose transport *via* an inhibition of Akt-regulated GLUT4 signaling in skeletal muscle cells. *Int J Mol Sci* 2021;**22**:7228.
63. Sarangadharan I, Regmi A, Chen YW, Hsu CP, Chen PC, Chang WH, et al. High sensitivity cardiac troponin I detection in physiological environment using AlGaN/GaN high electron mobility transistor (HEMT) Biosensors. *Biosens Bioelectron* 2018;**100**:282−9.
64. Li Y, Deng F, Goldys EM. A versatile CRISPR/Cas12a-based sensitivity amplifier suitable for commercial HRP-based ELISA kits. *Sensor Actuat B-Chem* 2021;**347**:130533.
65. Maiuri MC, Zalckvar E, Kimchi A, Kroemer G. Self-eating and self-killing: crosstalk between autophagy and apoptosis. *Nat Rev Mol Cell Biol* 2007;**8**:741−52.
66. Kroemer G, Marino G, Levine B. Autophagy and the integrated stress response. *Mol Cell* 2010;**40**:280−93.
67. Galluzzi L, Aaronson SA, Abrams J, Alnemri ES, Andrews DW, Baehrecke EH, et al. Guidelines for the use and interpretation of assays for monitoring cell death in higher eukaryotes. *Cell Death Differ* 2009;**16**:1093−107.
68. Marino G, Niso-Santano M, Baehrecke EH, Kroemer G. Self-consumption: the interplay of autophagy and apoptosis. *Nat Rev Mol Cell Biol* 2014;**15**:81−94.